ISIJ International, Vol. 55 (2015), No. 9, pp. 1994–2001

Heat Transfer Characteristics of a Pipe-laminar Jet Impinging on a Moving Hot Solid

Hitoshi FUJIMOTO,* Yamato SHIRAMASA, Kenta MORISAWA, Takayuki HAMA and Hirohiko TAKUDA

Graduate School of Energy Science, Kyoto University, Kyoto, 606-8501 Japan.

(*Received on March 4, 2015; accepted on May 18, 2015*)

This study experimentally investigated the hydrodynamics and heat transfer characteristics of a circular water jet impinging on a moving hot metal sheet as fundamental research on pipe-laminar cooling. The circular jet was issued from a 5-mm-diameter pipe nozzle. A 0.3-mm-thick sheet made of stainless steel was adopted as the test sheet. In the experiment, the liquid flow formed by the jet impingement was observed by flash photography, and the temperature profile on the underside of the moving sheet was measured by infrared thermography. The initial temperature of the moving solid was varied from 100°C to 500°C. The mean velocity at the nozzle exit ranged between 0.4 m/s and 1.2 m/s. The moving velocity of the solid was set to less than or equal to 1.5 m/s. The estimated heat flux profile on the cooled surface was found to be strongly dependent on the initial temperature of the sheet. When the initial temperature of the sheet was relatively low, a bow-shaped high heat flux region appeared in the upstream of the jet impact point. At higher temperatures, the heat flux area existed only in the jet impact regions. The heat flux increased with increasing initial sheet temperature, reached peak values, and then decreased drastically. The sharp decrease in the heat flux, which was due to the formation of a vapor layer, was influenced by the jet velocity and/or the sheet velocity.

KEY WORDS: pipe-laminar cooling; infrared thermography; flash photography; boiling heat transfer.

1. Introduction

Pipe-laminar jets are commonly utilized in runout-table (ROT) cooling in the hot rolling process in steel manufacturing industries. In this cooling, hot metal sheets are cooled by water jets from the final rolling temperature to a desired coiling temperature. The heat transfer from the metal sheet to the water jets is strongly dependent on the temperature of a solid associated with the boiling phenomena of the coolant. In the film boiling regime, in which the local temperature of the solid is high enough to stably form vapor layers between the solid surface and the coolant, the cooling rate of the solid is moderate. When the metal sheet is cooled below a certain temperature, breakage of the vapor layer occurs and the heat flux increases drastically. The temperature of the metal sheet also varies rapidly. In such a transient or strong nucleate boiling regime, precise control of the solid temperature is difficult.

The impact of a single water jet on a moving hot solid is a primary aspect of pipe-laminar cooling. The moving velocity of the solid is one of the parameters affecting the heat transfer characteristics. Several studies have been conducted on the heat transfer of a jet impinging on a moving solid. For example, Chen *et al.*[1] studied the heat transfer characteristics of an upward circular water jet onto a stationary or moving hot metal sheet. In their study, the initial plate temperature was up to 240°C and the moving velocity of the sheet was 0.5 m/s. Further, Gradeck *et al.*[2,3] studied quenching of a hot rotating cylinder with an initial temperature of 500–600°C by a subcooled water jet. Recently, Mozumder *et al.*[4] conducted experiments for investigating the quenching phenomena of a water jet impacting on a rotating cylinder at an initial temperature of 460–560°C. Vakili and Gadala[5] investigated the boiling heat transfer of multiple water jets impinging on a hot moving plate. In all these studies, the authors reported that the velocity of the moving solid influenced the heat transfer characteristics. However, the mechanism of jet impingement on a moving hot solid is still not very well understood.

In light of this background, in a previous study, the present authors investigated the heat transfer characteristics of a circular water jet impinging on a moving hot metal sheet[6] by varying the jet velocity and moving velocity of the solid as parameters. However, the temperature range of the solid (100–250°C) did not cover the film and transient boiling regimes. In the present study, this issue was resolved by conducting experiments at higher temperatures of up to 500°C of the solid.

The objective of the present study was to investigate the heat transfer characteristics of a circular jet impinging on a moving hot metal sheet. The test coolant was water at room temperature. The circular jet was issued from a 5-mm-diameter pipe nozzle. A 0.3-mm-thick sheet made of stainless steel was adopted as the test metal sheet. In the experiment, the liquid flow formed on the moving solid was

* Corresponding author: E-mail: h-fujimoto@energy.kyoto-u.ac.jp
DOI: http://dx.doi.org/10.2355/isijinternational.ISIJINT-2015-124

observed by flash photography. Further, the temperature profile on the underside of the moving sheet was measured by infrared thermography. The heat transfer characteristics were evaluated by solving the heat conduction equation through a finite volume method, by using the measured temperature profile as the boundary condition.

The initial temperature of the moving solid ranged between 100°C and 500°C, and the mean velocity at the nozzle exit ranged between 0.4 m/s and 1.2 m/s. Further, the moving velocity of the solid was set to 1.5 m/s. The effects of these parameters on the hydrodynamics and heat transfer process are discussed in detail in the paper.

2. Experiment

Figure 1 shows a schematic of the experimental apparatus. The experimental setup was modified slightly from that used in our previous work.[6] Furthermore, the measurement procedure and data reduction method were the same as those used in our previous work.[6] Thus, the experimental procedure is explained briefly here. The apparatus comprised a water supply system for producing a circular jet, a moving hot sheet mounted on a motor actuator, and observation equipment for performing flash photography and infrared thermography.

The test coolant was water at a temperature of approximately 17°C. The circular jet was issued vertically downward from a pipe nozzle having a diameter of 5.0 mm and length of 500 mm. The mean jet velocity V_0 at the nozzle exit was set as 0.4, 0.8, or 1.2 m/s.

The test sheet, made of stainless steel SUS430, was initially set away from the test section. It was electrically heated with a DC power supply. At every run, the linear motor actuator with the test sheet was activated after the electric power supply to the sheet was cut. The uniformly heated test sheet went into the test section at a moving velocity V_s of 0.5, 1.0, or 1.5 m/s, and impingement of the circular jet on the sheet occurred. The nozzle-to-plate spacing was set to 40 mm. Furthermore, the initial temperature of the test sheet was in the range of 100–500°C.

The test sheet was 60 mm wide, 220 mm long, and 0.3 mm thick, as shown in **Fig. 2**. Its two long sides were bent downward at a right angle at a point 5 mm from the edge in order to prevent unwanted deformation of the sheet during the experiments. The underside of the sheet was coated with black body paint with an emissivity of 0.94 for accurate measurement of temperature by infrared thermography. A pair of K-type thermocouples with a wire diameter of 0.3 mm was spot-welded on the underside of the sheet to measure the local temperature and to calibrate the temperature measurement with the results of the infrared thermography. An infrared camera with a resolution of 320×240 pixels at 60 fps was set to face vertically upward, with a camera-to-sheet distance of approximately 300 mm, as shown in **Fig. 3**.

Two digital cameras were used to observe the motion of the liquid film. One was placed above the test sheet and

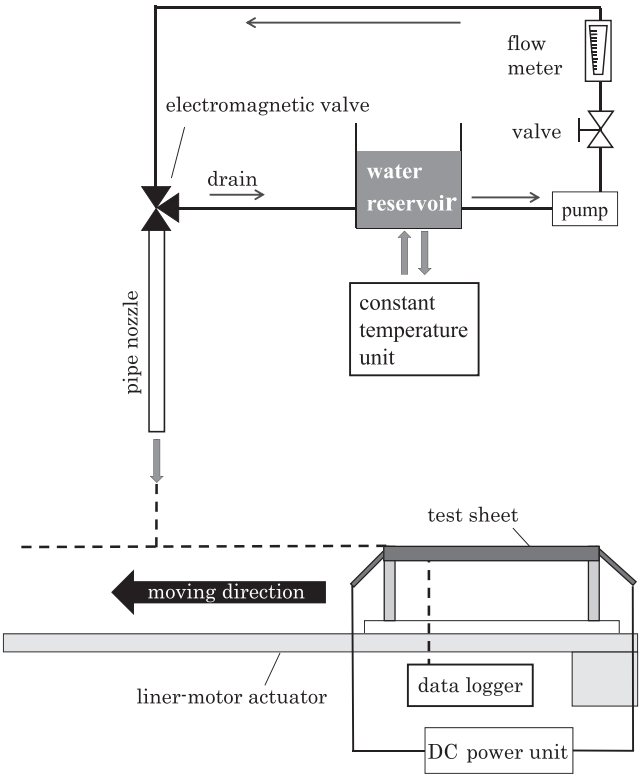

Fig. 1. Schematic diagram of experimental apparatus.

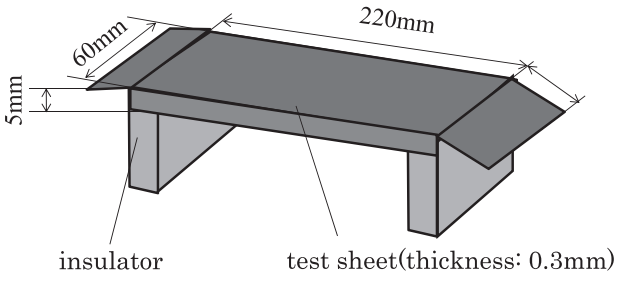

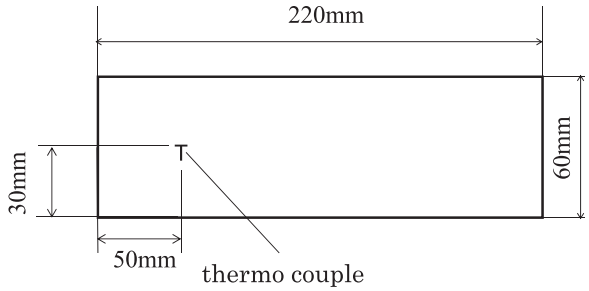

Fig. 2. Dimensions of test sheet attached to insulator.

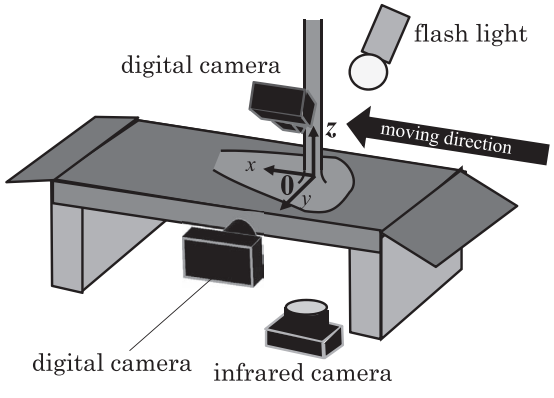

Fig. 3. Schematic diagram of flash photography and infrared thermography.

the other was placed beside the test sheet. A strobe light with a light duration of less than 2 μs was used as the light source. The cameras were adjusted to expose the images of the liquid film only when the strobe light was triggered. Activation of the flash light and the temperature measurement by thermography were conducted after the liquid film was stably formed on the moving test sheet.

To evaluate the local temperature profile as well as the heat flux on the top surface of the sheet, the inverse heat conduction problem was solved numerically using the measured temperature profile on the underside of the sheet. The heat conduction equation inside the sheet in the three-dimensional Cartesian coordinate system is given by

$$\rho_p c_p \left(V_s \frac{\partial T}{\partial x} \right) = \lambda_p \left(\frac{\partial^2 T}{\partial x^2} + \frac{\partial^2 T}{\partial y^2} + \frac{\partial^2 T}{\partial z^2} \right), \quad \text{..... (1)}$$

where T is the local temperature of the sheet; and ρ_p, C_p, and λ_p denote the material density, specific heat, and thermal conductivity, respectively. The coordinates (x,y,z) are defined as shown in Fig. 3. The origin was set to the jet impact point on the wet surface. The temperature profile was assumed to be steady in the coordinate system. Equation (1) was solved numerically by using the finite volume approximation developed by Vader *et al.*[7] A rectangular computer domain with a length of 79.1 mm, width of 50.9 mm, and thickness of 0.3 mm was divided into 140×90×200 cells in the *x*-, *y*-, and *z*-directions. The material properties were given by the network database system for thermophysical property data provided by National Institute of Advanced Industrial Science and Technology (AIST) in Japan. Temperature dependence of the material properties was taken into account. More information on the data reduction method and the experimental procedure is available in our previous paper.[6]

3. Results and Discussion

3.1. Preliminary Experiments: Impinging Jet on a Stationary Solid

The heat transfer characteristics of a circular jet impinging on a stationary solid surface have been investigated since many decades. Furthermore, theoretical and empirical correlations capable of predicting heat transfer characteristics in steady state have been proposed[8–11] under conditions that the temperature of the solid is below the boiling temperature of the liquid and the heat flux from the solid to the liquid is constant. In order to validate the present experimental procedure and data reduction method, experiments were conducted in this study under such conditions and the obtained data were compared with the correlations.

A test sheet 25 mm wide, 120 mm long, and 0.3 mm thick was used for the preliminary experiments, as shown in **Fig. 4**. The test sheet was statically set below the pipe nozzle so that water jet always impinged on the same point. The sheet was heated electrically with a preset power to maintain a "constant heat flux condition" throughout the experiment. A pair of copper probes was spot-welded at 50-mm intervals along the centerline of the opposite surface in order to monitor the voltage drop between these two points with a data logger. The steady-state temperature profile on the rear side

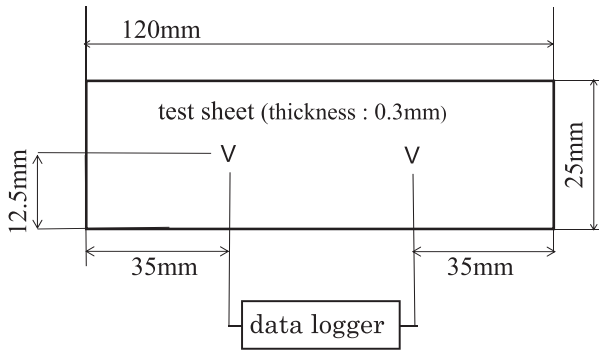

Fig. 4. Dimensions of test sheet for preliminary experiment.

was measured with an infrared camera.

The temperature profile in the test sheet was computed by solving the following heat conduction equation by a method similar to that explained in the previous section:

$$\lambda_p \left(\frac{\partial^2 T}{\partial x^2} + \frac{\partial^2 T}{\partial y^2} + \frac{\partial^2 T}{\partial z^2} \right) + \dot{q} = 0, \quad \text{..... (2)}$$

where $\dot{q}$ denotes the heat source resulting from electric heating.

Some correlations for predicting the stagnation Nusselt number have been formulated under the conditions of a uniform, laminar velocity profile of a circular jet. Wang *et al.*,[8] Liu *et al.*,[9] and Zhao and Ma[10] proposed the following equations:

$$\left.\begin{aligned} Nu_j &= 0.717\,\mathrm{Re}_j^{0.5}\,\mathrm{Pr}^{0.37}, \quad 0.5 \le \mathrm{Pr} \le 50 \\ Nu_j &= 0.797\,\mathrm{Re}_j^{0.5}\,\mathrm{Pr}^{1/3}, \quad \mathrm{Pr} > 3 \\ Nu_j &= 0.7212\,\mathrm{Re}_j^{0.5}\,\mathrm{Pr}^{0.37}, \quad 3.0 \le \mathrm{Pr} < 10.0 \end{aligned}\right\} \quad \text{..... (3)}$$

where Nu_j, Re_j, and Pr are the stagnation Nusselt number, jet Reynolds number, and Prandtl number, respectively. Nu_j and Re_j are defined on the basis of the jet velocity V_j just before impact and the jet diameter D_j as

$$Nu_j = \frac{qD_j}{(T_w - T_f)\lambda_f} \text{ and } \mathrm{Re}_j = \frac{D_j V_j}{\nu_f}, \quad \text{..... (4)}$$

where q, λ_f, ν_f, T_w and T_f denote the heat flux, thermal conductivity of water, kinematic viscosity coefficient of water, local temperature of the wet surface, and temperature of water, respectively. D_j and V_j were calculated using a simple mass conservation law as

$$D_j = D\sqrt{\frac{V_0}{V_j}}, \quad V_j = \sqrt{V_0^2 + 2gH}, \quad \text{..... (5)}$$

where D, V_0, g, and H are the inner diameter of the nozzle, mean coolant velocity at the nozzle exit, gravitational acceleration, and the nozzle-to-plate spacing, respectively.

Figure 5(a) shows a comparison of the present experimental data with these correlations for a heat flux of 0.315 MW/m^2. The measured stagnation Nusselt number increased with increasing jet Reynolds number. The experimental data agreed moderately with the correlations but were larger than the predictions. This discrepancy between the experimental data and the predictions was caused by the

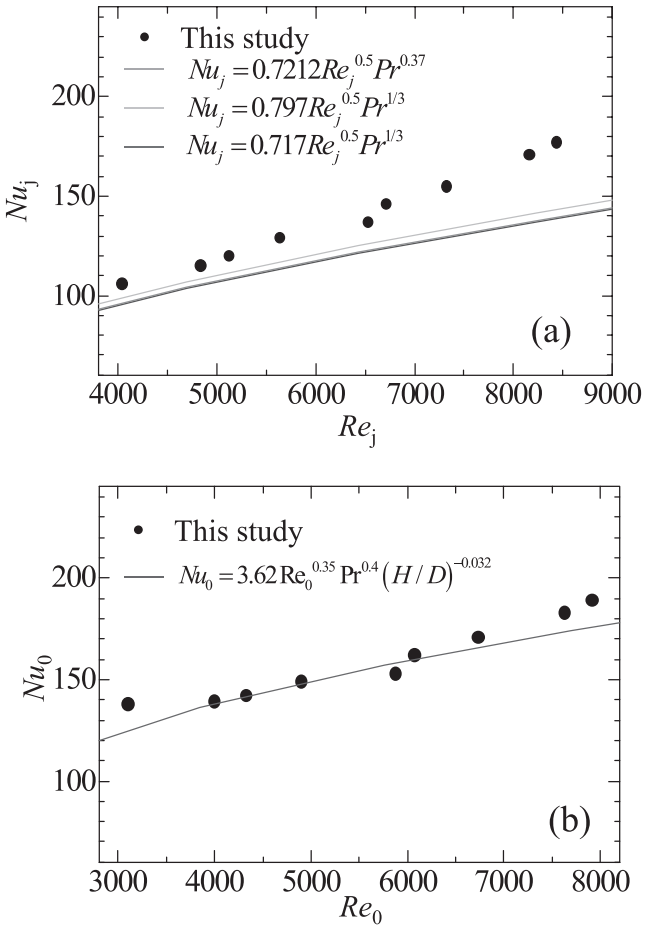

Fig. 5. Comparison of measured stagnation Nusselt numbers with correlations proposed by other researchers.

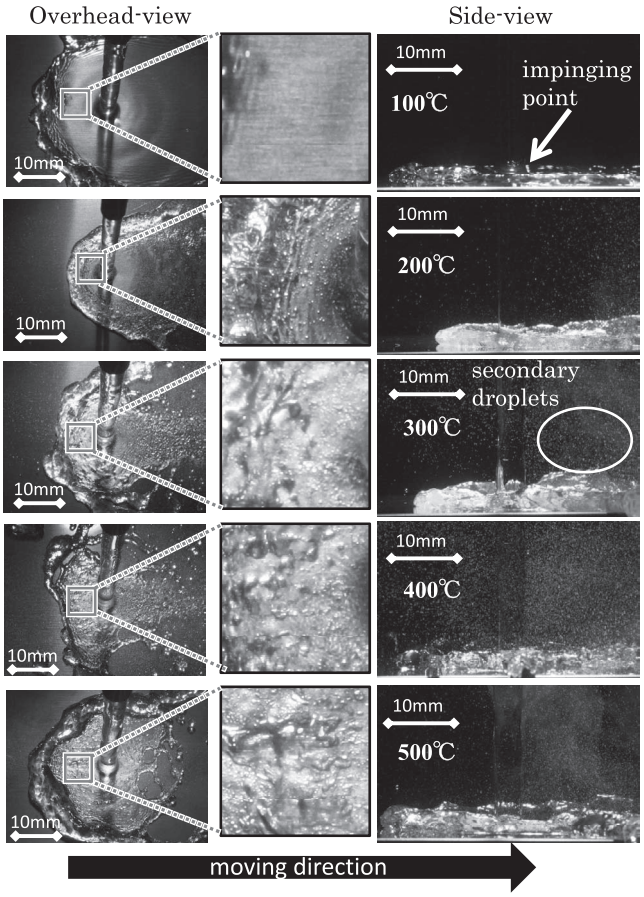

Fig. 6. Observed film flow for varying initial temperatures of sheet—T_s=100, 200, 300, 400, and 500°C—under conditions of V_0=0.8 m/s and V_s=1.0 m/s.

difference in velocity profiles. That is, the correlations were obtained by assuming a uniform, laminar velocity profile; however, the jet was a fully developed turbulent flow in the experiments, wherein the local jet velocity is large at the center and decreases radially outward.

Stevens and Webb[11] experimentally studied the local heat transfer in the case of axisymmetric, single-phase liquid jets impinging on a constant heat flux surface and proposed an empirical correlation of the stagnation point Nusselt number. They adopted a long pipe nozzle with a diameter of 5.8 mm, which was similar to that in the present experiments (=5 mm). Their correlation was defined as

$$Nu_0 = 3.62\,\mathrm{Re}_0^{0.35}\,\mathrm{Pr}^{0.4}(H/D)^{-0.032}, \quad \text{..... (6)}$$

where the Reynolds and Nusselt numbers are respectively defined as

$$\mathrm{Re}_0 = \frac{DV_0}{\nu_f} \text{ and } Nu_0 = \frac{qD}{(T_w - T_f)\lambda_f}. \quad \text{..... (7)}$$

The present experimental data showed the best fit to Eq. (6), as shown in Fig. 5(b). It was concluded from the above results that the present experiments could provide feasible results.

3.2. Effect of Varying Initial Sheet Temperature

Figure 6 shows photographs of the film flows formed by the impingement of the water jet for a jet velocity of V_0=0.8 m/s and sheet velocity of V_s=1.0 m/s. The initial temperature of the solid as a parameter was varied. The left column in the figure contains overhead-view images of the flow formed by the jet impingement. Photographs in the middle column are magnified images of the rectangular areas in the left column. The right column contains side-view images of the flow. Each pair of overhead- and side-view images was taken simultaneously. At T_s=100°C (first row in the figure), a thin liquid film was formed near the impact point. A bow-shaped hydraulic jump was observed on the upstream side of the jet impact point. Very few bubbles were seen in the magnified photographs in the middle column. At T_s=200°C (second row), a smooth bow-shaped hydraulic jump was seen. Boiling vapor bubbles were present at the liquid/solid interface, as seen in the magnified figure. At T_s=300, 400, and 500°C, the liquid film in the middle-column photographs appeared hazy because of the presence of numerous vapor bubbles or a vapor film. Further, local breakage of the liquid film occurred in the downstream region owing to strong boiling. At T_s=300°C, numerous secondary droplets were jetted upward from the liquid film, as seen in the side-view image. These were formed by the bursting of the boiling vapor bubbles. At T_s=400°C, secondary droplets were observed in not only the downstream region but also the upstream region of the jet impact point. At T_s=500°C, fewer secondary droplets than those in the case of T_s=400°C were formed, suggesting that the vapor film, instead of bubbles, was stably present between the liquid and the solid surface.

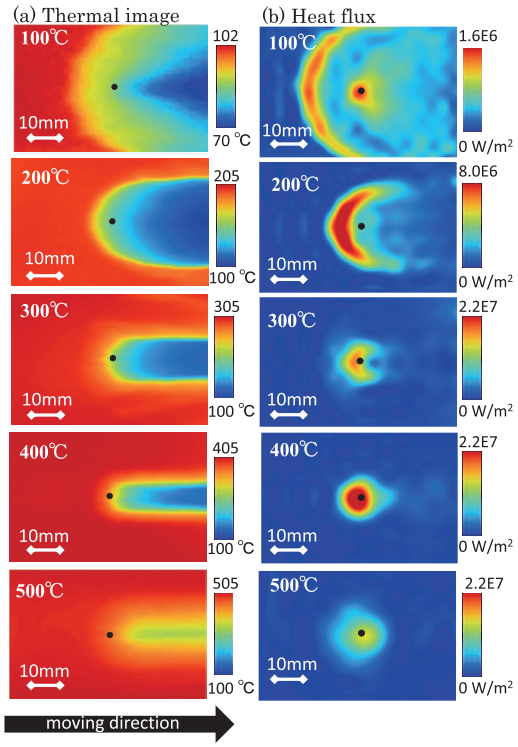

Fig. 7. (a) Thermal images captured by infrared camera and (b) estimated local heat flux on wet surface for T_s=100, 200, 300, 400, and 500°C under conditions of V_0=0.8 m/s and V_s=1.0 m/s.

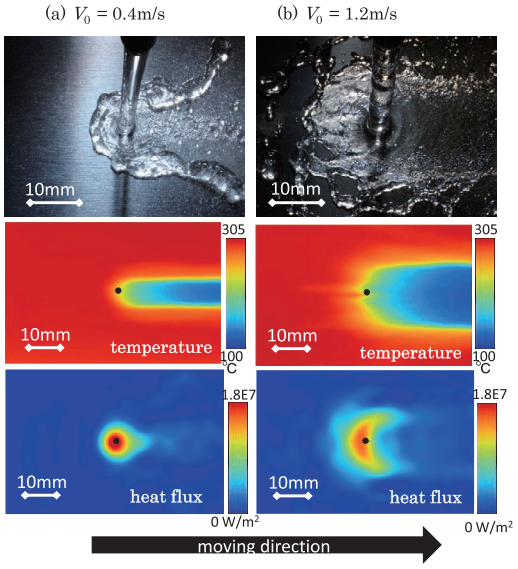

Fig. 9. Observed film flows, thermal images captured by infrared camera, and distribution of estimated local heat flux on wet surface for (a) V_0=0.4 m/s and (b) V_0=1.2 m/s under conditions of V_s=1.0 m/s and T_s=300°C.

Figure 7(a) shows the thermal images on the underside as captured by the infrared camera, and Fig. 7(b) shows the distributions of the estimated heat flux at the cooled surface obtained by solving the inverse heat conduction problem. The experimental conditions were the same as those in the previous experiments whose results are shown in Fig. 6. It should be noted that the color key (legend) varied depending on the conditions. Further, the black points in each image in Fig. 7 indicate the positions of jet impact (x= y= 0 mm), as

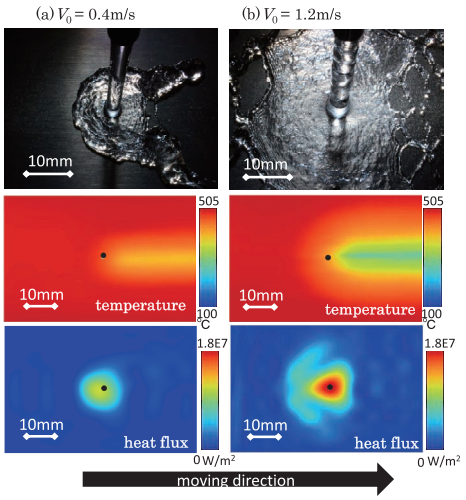

Fig. 10. Observed film flows, thermal images captured by infrared camera, and distribution of estimated local heat flux on wet surface for (a) V_0=0.4 m/s and (b) V_0=1.2 m/s under conditions of V_s=1.0 m/s and T_s=500°C.

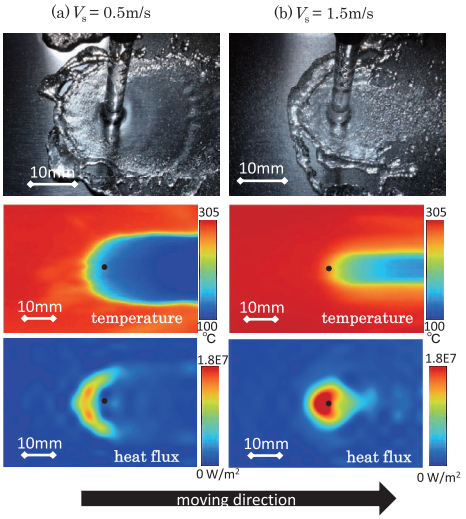

Fig. 12. Observed film flows, thermal images captured by infrared camera, and distribution of estimated local heat flux on wet surface for (a) V_s=0.5 m/s and (b) V_s=1.5 m/s, under conditions of V_0=0.8 m/s and T_s=300°C.

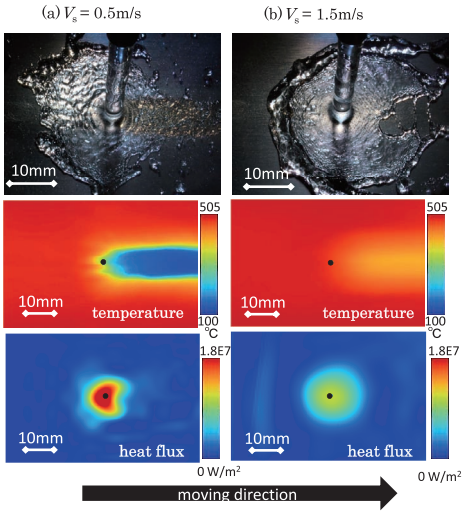

Fig. 13. Observed film flows, thermal images captured by infrared camera, and distribution of estimated local heat flux on wet surface for (a) V_s=0.5 m/s and (b) V_s=1.5 m/s, under conditions of V_0=0.8 m/s and T_s=500°C.

defined in Fig. 3. In (a), the low-temperature area was apparently reduced in size with increasing initial temperature of the solid. A comparison of Figs. 6 with 7(a) shows that the low-temperature areas coincided roughly with the wet areas (apparent liquid/solid contact areas) for T_s=100 and 200°C, but they did not coincide in the temperature range of T_s=300–500°C.

It was found from Figs. 6 and 7(b) that for T_s=100°C, the heat flux was large in both the hydraulic jump region and the jet impact region. In the hydraulic jump region, where the first liquid/solid direct contact occurs, the temperature difference between the liquid and the solid is large. In the jet impact region, low-temperature coolant is continuously supplied by the jet impingement. As a consequence, the heat flux is high in these regions. For T_s=200°C, the heat flux was high in the bow-shaped hydraulic jump region. For T_s=300, 400, and 500°C, effective cooling areas were present only in the jet impact region. In other regions covered with the liquid film, the heat flux was not too high, because vapor bubbles and/or a vapor film was formed between the liquid and the solid surface, or local breakage of the liquid film occurred as shown in Fig. 6. The high heat flux area was bow-shaped at T_s=300°C and circular-shaped at T_s=400°C. At T_s=500°C, the heat flux in the jet impact region was appreciably smaller than that at T_s=400°C.

To clearly understand the effect of varying the initial temperature of the test sheet on the heat transfer characteristics, the maximum heat flux was plotted at various temperatures for V_0=0.8 m/s and V_s=1.0 m/s, as shown in **Fig. 8**(a). It should be noted that the position at which the maximum heat flux was observed varied with the temperature of the solid, as shown in Fig. 7. For T_s=100–250°C, the maximum heat flux appeared in the hydraulic jump region. For T_s=300–500°C, the maximum heat flux appeared in the vicinity of the jet impinging point. In the range of T_s=100–400°C, the maximum heat flux increased monotonically with increasing initial temperature of the sheet. It reached a peak at approximately T_s=400°C and decreased at higher temperatures.

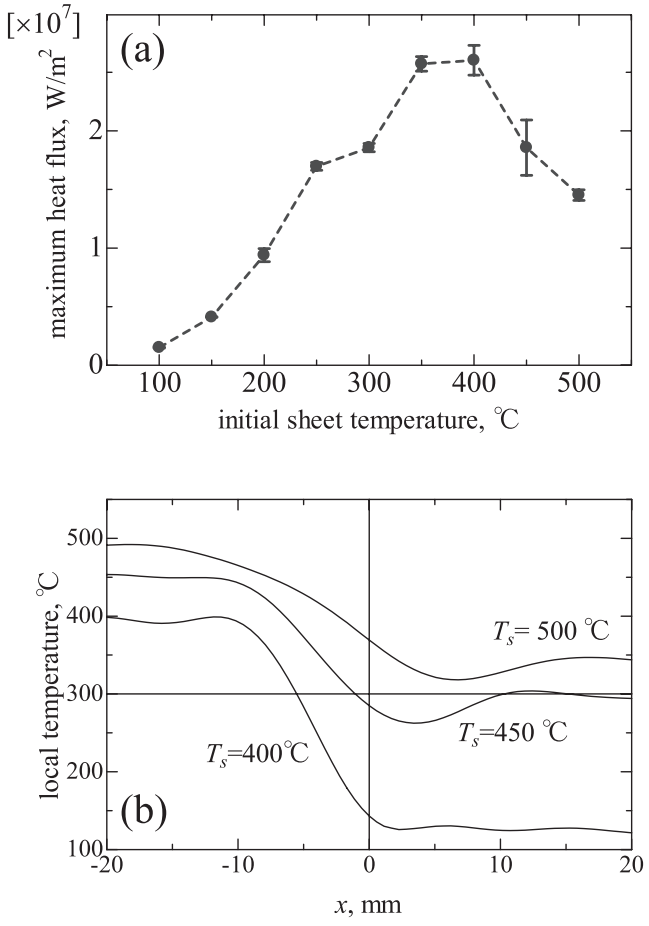

Fig. 8. (a) Maximum heat flux at various initial temperatures of sheet for V_0=0.8 m/s and V_s=1.0 m/s and (b) calculated temperature distribution on wet surface along movement direction via the impact point.

The sharp decrease in the maximum heat flux between T_s=400°C and T_s=450°C was caused by the formation of a vapor layer in the jet impact region, which prevented direct contact between the coolant and the solid. The critical boundary corresponding to sharp decrease in the maximum heat flux can be explained by the relationship between the local temperature of the solid surface and the limit of superheat of the coolant. When the liquid is heated above the limit of superheat, phase transition from the liquid phase to the vapor phase occurs very rapidly owing to homogeneous nucleation boiling. Coalescence of numerous bubbles results in the formation of a vapor film around the heat source in a very short time. According to the literature,[12–15] the limit of superheat of water at atmospheric pressure is approximately 300°C. Figure 8(b) shows the temperature distributions of the wet surface along the movement direction of the sheet via the jet impact point (x=y=0 mm, as defined in Fig. 3) for T_s=400, 450, and 500°C under the conditions of V_0=0.8 m/s and V_s=1.0 m/s. For T_s=450 and 500°C, the calculated surface temperature was roughly equal to or higher than the superheat limit of water (~300°C) at x=0 mm, whereas the local temperature in the jet impact region was appreciably lower than the superheat limit for T_s=400°C. It is considered that the vapor layer was formed at T_s=450 and 500°C. In contrast, liquid was in effective contact with the moving solid at T_s=400°C. Similar results were obtained under conditions of other jet velocities and/or other moving velocities of the sheet.

In the present study, the initial temperature ranged up to 500°C because of the limitation of the experimental setup. It is postulated that at much higher ranges of the initial temperature, the maximum heat flux increases again with increasing initial temperatures.

3.3. Effect of Varying Jet Velocity

Figures 9(a) and 9(b) show the observed film flows, measured temperature profiles on the rear surface, and estimated heat flux distributions on the wet surface for V_0=0.4 m/s and V_0=1.2 m/s, respectively, under the conditions of V_s=1.0 m/s and T_s=300°C. The liquid film expanded more widely for a larger jet velocity, which is associated with the higher impact inertia of the jet. Furthermore, the low-temperature area spread more widely at a larger jet velocity. The high heat flux area was small and circular-shaped for (a) V_0=0.4 and bow-shaped for (b) V_0=1.2 m/s.

Figures 10(a) and 10(b) show the results for jet velocities of V_0=0.4 m/s and V_0=1.2 m/s, respectively, at V_s=1.0 m/s and T_s=500°C. The high heat flux area was

wider for a larger jet velocity.

Figure 11 shows the distribution of the maximum heat flux for V_0=0.4, 0.8, and 1.2 m/s, under the condition of V_s=1.0 m/s, where the temperature of the solid as a parameter was varied. In all cases, the maximum heat flux increased with the initial temperature of the solid, reached peak values, and then decreased. In the temperature range of 100–250°C, the positions of the peak heat flux were located in the hydraulic jump region and the maximum heat fluxes were very similar regardless of the jet velocity. For the temperatures of 250, 300 and 350°C, the peak heat flux for V_0=1.2 m/s was smaller than the results of smaller jet velocities. This does not mean that the solid was cooled effectively for a smaller jet velocity. As can be seen in Fig. 9, the high heat flux area for V_0=1.2 m/s was much wider than that for V_0=0.4 m/s. The total heat transfer obtained by integrating the local heat flux over the entire wet surface was apparently larger for V_0=1.2 m/s. It is necessary to remember that the maximum heat flux is not a parameter representing the total heat flux from the moving sheet to the coolant.

The temperature at which a peak heat flux was observed was higher for larger jet velocity on account of the jet impact inertia. In addition, the peak of the maximum heat flux increased slightly with increasing mean jet velocity.

3.4. Effect of Varying Sheet Velocity

Figures 12(a) and 12(b) show the liquid flow, thermal image at the rear surface, and distributions of the estimated heat flux at the wet surface for V_s=0.5 m/s and V_s=1.5 m/s, respectively, under the conditions of V_0=0.8 m/s and T_s=300°C. In (a), the liquid film spread widely and the low-temperature area coincided roughly with the apparent wet region. A bow-shaped high heat flux area existed in the upstream of the jet impingement point. In (b), the liquid film and low-temperature areas were smaller than those in (a). The liquid film was locally broken in the downstream region owing to the blowout of vapor bubbles. A circular high heat flux area was seen in the jet impingement region.

Figures 13(a) and 13(b) show the results for V_s=0.5 m/s and V_s=1.5 m/s, respectively, under the conditions of V_0=0.8 m/s and T_s=500°C. In (a), the high heat flux area was present in the jet impact region and the low-temperature area was seen in the downstream region. In (b), the heat flux in the jet impact region was not as high as that in (a). The temperature of the sheet was maintained high, suggesting that the vapor film was formed stably.

The sheet velocity can be related to the duration of impact of the liquid jet and the hot solid. When the metal sheet is unmoved, the water jet always impinges on the same point on the solid surface and the local temperature of the solid decreases with the passage of time. In the case that the sheet is moving, impingement of the liquid jet at a certain point on the solid occurs in a short period. The hot metal sheet moves into the jet impact region continuously. Because the impingement time decreases with increasing sheet velocity, the decrease in local temperature of the solid is smaller for a larger sheet velocity. Thus, the moving velocity of the sheet is seen to have a strong influence on the heat transfer characteristics in the jet impingement region.

Figure 14 shows the distribution of the maximum heat flux for V_s=0.5, 1.0, and 1.5 m/s under the condition of V_0=0.8 m/s, where the temperature of the solid as a parameter is varied. The temperature at which the peak of the maximum heat flux occurred was lower for a larger sheet velocity, because the local temperature of the sheet was maintained at high values. At V_s=0.5 m/s, a sharp decrease

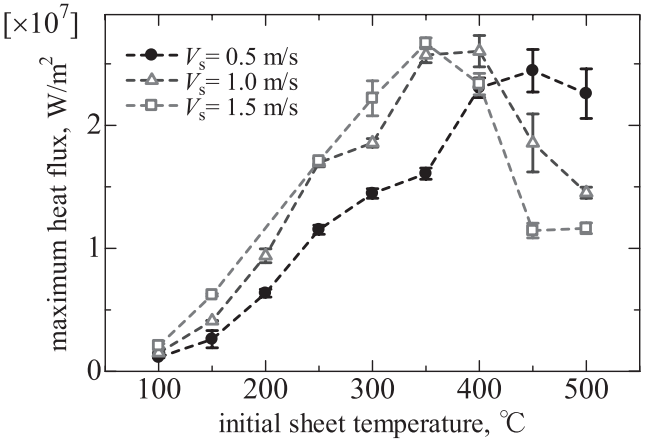

Fig. 14. Effect of varying sheet velocity on maximum heat flux for V_0= 0.8 m/s.

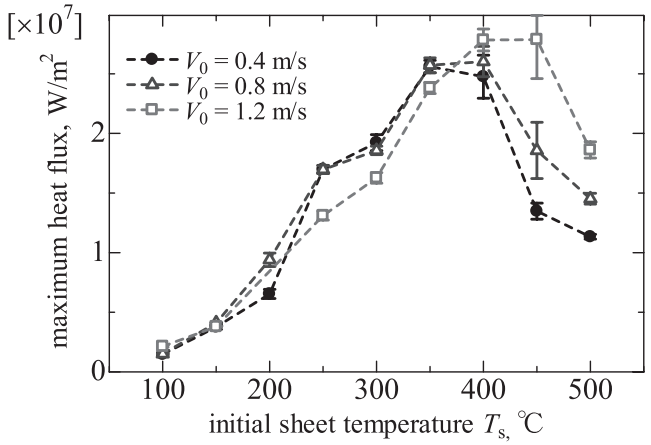

Fig. 11. Effect of varying mean jet velocity on distribution of maximum heat flux for V_s=1.0 m/s.

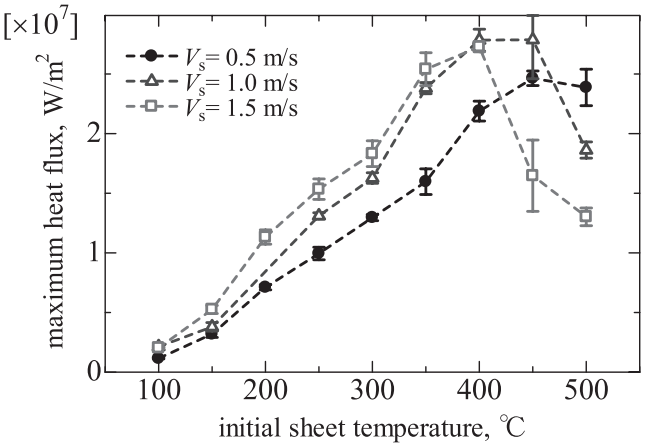

Fig. 15. Effect of varying sheet velocity on distribution of maximum heat flux for V_0=1.2 m/s.

in the maximum heat flux did not occur even at T_s=500°C. Similar trends were obtained under other jet velocity conditions, as shown in **Fig. 15**.

4. Conclusions

The hydrodynamics and heat transfer characteristics of a circular water jet impinging on a heated moving surface were investigated experimentally. The main results obtained in this study are summarized below.

(1) The heat flux distribution was strongly dependent on the initial temperature of the solid. When the temperature of the solid was relatively low, a bow-shaped high heat flux area was observed to have formed in the upstream of the jet impact point. The low-temperature area of the sheet coincided moderately with the wet region. At higher sheet temperatures, a high heat flux region was present only in the jet impact region. In other regions covered with the liquid film, the vapor bubbles or vapor layer prevented direct contact between the liquid and the solid. As a consequence, the heat flux was not as high there.

(2) The maximum heat flux increased with increasing initial temperature of a moving solid, reached peak values, and then decreased sharply. The sharp decrease in the maximum heat flux was caused by the formation of a vapor layer in the jet impact region. In such a case, the local temperature of the solid was roughly equal to or higher than the limit of superheat of the liquid.

(3) The temperature at which the peak of the maximum heat flux occurred varied depending on the jet velocity and/or the sheet velocity. The temperatures increased with an increase in the jet velocity and decrease in the sheet velocity.

REFERENCES

1) S.-J. Chen, J. Kothari and A. A. Tseng: *Exp. Thermal Fluid Sci.*, **4** (1991), 343.
2) M. Gradeck, A. Kouachi, M. Lebouche, F. Volle, D. Maillet and J. L. Borean: *Int. J. Heat Mass Transf.*, **52** (2009), 1094.
3) M. Gradeck, A. Kouachi, J. L. Borean, P. Gardin and M. Lebouche: *Int. J. Heat Mass Transf.*, **54** (2011), 5527.
4) A. K. Mozumder, Y. Mitsutake and M. Monde: *Int. J. Heat Mass Transf.*, **68** (2014), 466.
5) S. Vakili and M. S. Gadala: *Heat Transfer Eng.*, **34** (2013), 580.
6) H. Fujimoto, K. Tatebe, T. Hama and H. Takuda: *ISIJ Int.*, **54** (2014), 1338.
7) D. Vader, F. P. Incropera and R. Viskanta: *Exp. Thermal Fluid Sci.*, **4** (1991), 1.
8) X. S. Wang, Z. Dagan and L. M. Jiji: *Int. J. Heat Mass Transf.*, **32** (1989), 1361.
9) X. Liu, J. H. V. Lienhard and J. S. Lombara: *J. Heat Transf.*, **113** (1991), 571.
10) H. Y. Zhao and C. F. Ma: *J. Heat Transf.*, **5** (1996), 272.
11) J. Stevens and B. W. Webb: *J. Heat Transf.*, **113** (1991), 71.
12) V. P. Skripov: Metastable Liquids, John Wiley and Sons, New York, (1974), 83.
13) J. H. Lienhard: *Chem. Eng. Sci.*, **31** (1976), 847.
14) C. T. Avedisian: *J. Phys. Chem. Data*, **14** (1985), 695.
15) C. T. Avedisian, W. S. Osborne, F. D. Mcleod and C. M. Curley: *Proc. R. Soc. A*, **455** (1999), 3875.